Spatially-Adaptive Multi-Scale Optimization for Local Parameter Estimation: Application in Cardiac Electrophysiological Models

Jwala Dhamala[1], B. Milan Horacek[2], John L. Sapp[2], and Linwei Wang[1]

[1]Rochester Institute of Technology, Rochester, NY, USA
[2]Dalhousie University, Halifax, NS, Canada

Abstract. The estimation of local parameter values for a 3D cardiac model is important for revealing abnormal tissues with altered material properties and for building patient-specific models. Existing works in local parameter estimation typically represent the heart with a small number of pre-defined segments to reduce the dimension of unknowns. Such low-resolution approaches have limited ability to estimate tissues with varying sizes, locations, and distributions. We present a novel optimization framework to achieve a higher-resolution parameter estimation without using a highe number of unknowns. It has two central elements: 1) a multi-scale coarse-to-fine optimization that uses low-resolution solutions to facilitate the higher-resolution optimization; and 2) a spatially-adaptive scheme that dedicates higher resolution to regions of heterogeneous tissue properties whereas retaining low resolution in homogeneous regions. Synthetic and real-data experiments demonstrate the ability of the presented framework to improve the accuracy of local parameter estimation in comparison to optimization based on fixed-segment models.

Keywords: Parameter estimation; Cardiac electrophysiological model; Multi-scale optimization; Gaussian Process.

1 Introduction

Many cardiac diseases stem from abnormal myocardial tissues with altered material properties. The quantitative knowledge about these abnormal tissues is paramount to the diagnosis, treatment, and prevention of relevant cardiac diseases. Since it is difficult to directly measure the material property of cardiac tissues, one effective way to quantify pathological tissue properties is to estimate the three-dimensionally distributed parameters of a cardiac model using indirect measurement data. This will in addition provide a patient-specific model useful for personalized treatment planning and prognosis [4].

Much effort has been reported on parameter estimation for complex physiological models. For example, derivative-free optimization methods [9] are shown to be effective in handling the complex objective functions in these problems. Alternatively, surrogate models such as spectral representation based on polynomial chaos [4], multivariate polynomial regression model [10], and Gaussian process model [5] have gained increasing interest in recent years.

Nevertheless, progress has been limited in estimating local parameters that are three-dimensionally distributed in space. Many works focus on the estimation of global parameters [5] by assuming uniform tissue property throughout the myocardium. Although it provides a fast calibration of a patient-specific model, global parameter estimation does not reveal the local change of tissue properties. Toward local parameter estimation, a commonly-used approach is to divide the myocardium into a set of pre-defined segments and assume the parameter to be uniform within each segment. This substantially reduces the dimension of unknowns (to a range of 3 to 27) [9, 10], yet the resolution is too low to capture abnormal tissues with different sizes, locations, and distributions. Moreover, as the number of segments increases, a good initialization becomes critical [9] which typically requires additional data to delineate diseased regions *a priori*. A critical gap remains between the need for a high-resolution local parameter estimation and the difficulty to accommodate high-dimensional optimization.

To bridge this gap, we propose a novel framework to go beyond fixed low-resolution parameter estimation without invoking an infeasible number of unknowns. This is achieved via two primary elements. First, a multi-scale hierarchy is used to progressively use low-resolution results to facilitate higher-resolution optimization, thereby alleviating the issue of identifiability. Second, instead of uniform resolution in space, an adaptive scheme is used to selectively allocate higher resolution in heterogeneous regions whereas retaining lower resolution in homogeneous regions. This multi-scale, spatially-adpative framework is developed with Gaussian Process (GP) based optimization [7]. It shares an important intuition with [1] where non-uniform mesh subdivision is used in parameter estimation, although with fundamental differences in the coarser-to-fine transition of information and the motivation (tissue heterogeneity) for adaptive resolution.

The proposed framework is applied to local parameter estimation for a 3D cardiac electrophysiological (EP) model using non-invasive electrocardiographic (ECG) data. It is noteworthy that the remote global ECG data increase the difficulty in identifying local tissue properties in comparison to local direct mapping data. The presented method is tested on a set of synthetic and real-data experiments. In comparison to the derivative-free BOBYQA [6] method carried out on a predefined 18-segment model, the presented method demonstrates higher accuracy in local parameter estimation using a similar or even fewer number of unknowns. While the presented framework is reported here with GP based optimization, it can accommodate other standard optimization methods. It is also applicable to local parameter estimation beyond cardiac EP models.

2 Cardiac Electrophysiology and ECG

The relationship between latent cardiac electrophysiological properties and body-surface ECG can be described with the following two models.

2.1 Cardiac Electrophysiological Model: The spatiotemporal evolution of cardiac action potential can be described by a set of differential equations, ranging from complex ionic models with tens of hundreds of parameters to simpler models with a few parameters [2]. As an initial demonstration of feasibility for

the proposed framework, we consider parameter estimation for the two-variable *Aliev-Panfilov* (AP) [2] model because of its ability to simulate electrical dynamics of the heart with a small number of parameters and reasonable computation.

$$\begin{aligned} \partial u/\partial t &= \partial/\partial x_i d_{ij} \partial u/\partial x_j - ku(u-a)(u-1) - uv \\ \partial v/\partial t &= \varepsilon(u,v)(-v - ku(u-a-1)). \end{aligned} \tag{1}$$

Here, u is the transmembrane action potential and v is the recovery current. Parameter d_{ij} is the spatial conductivity, ε controls the coupling between the recovery current and action potential, k controls the repolarization, and a controls the excitability of a cell. In this study, we focus on parameter a because it is one of the most sensitive parameter of the model and its value is documented to be closely associated with the ischemic severity of the myocardial tissue [2]. The meshfree method is used to discretize and solve (1) on the 3D myocardium [8], with an approximate resolution of 6-mm ($\sim 10^3$ nodes).

2.2 ECG Measurement Model: Cardiac action potential produces potential on the body surface that is measured as time-varying ECG signals. This measurement process can be described by the quasi-static approximation of the electromagnetic theory [8]. Solving this governing equation on the discrete mesh of heart and torso models specific to an individual, a linear model between ECG data $\mathbf{\Phi}$ and transmural action potential $\mathbf{u}$ can be obtained as: $\mathbf{\Phi} = \mathbf{H}\mathbf{u}$ [8].

3 Spatially-Adaptive, Multi-Scale Optimization

Estimation of the three-dimensionally distributed tissue excitability $\mathbf{a}$ from ECG data $\mathbf{y}$ can be formulated as a bound-constrained global maximization problem:

$$\max_{l \le \mathbf{a} \le u} G(\mathbf{a}) = \max_{l \le \mathbf{a} \le u} \sum_{i=1}^{L} \Big(\frac{\sum_{t=1}^{M} (y_{it} - \bar{y}_i)(\Phi_{it} - \bar{\Phi}_i)}{\sqrt{\sum_{t=1}^{M} (y_{it} - \bar{y}_i)^2 \sum_{t=1}^{M} (\Phi_{it} - \bar{\Phi}_i)^2}} - \sum_{t=1}^{M} (\Phi_{it} - y_{it})^2 \Big). \tag{2}$$

where $\mathbf{\Phi} = f(\mathbf{a})$ is a composite of the measurement and AP models described in section 2. The objective function (2) includes both a correlation coefficient and a squared error to balance the morphology and magnitude similarity between the ECG data $\mathbf{y}$ and the model output. L represents the number of ECG leads.

The direct estimation of $\mathbf{a}$ requires a high-dimensional optimization (at the order of 10^3) that is not feasible due to both identifiability and computation issues. To achieve high-resolution local parameter estimation, the optimization framework described below includes two key components: 1) a hierarchical coarse-to-fine estimation, and 2) a spatially-adaptive resolution that is refined at regions of heterogeneity. This framework is developed with GP-based optimization.

3.1 Multi-Scale Hierarchy: A coarse-to-fine optimization has the advantage to use lower-resolution solution to reduce the search space of higher-resolution optimizations. To facilitate this, we construct a multi-scale representation of the cardiac mesh using Agglomerative hierarchical clustering [3], exploiting the spatial smoothness of tissue properties. A partial tree structure of this multi-scale model can be seen in Fig. 1. The clustering starts with each node in the cardiac

mesh as a separate cluster. Every two closest clusters, based on the Euclidean distance and linkage metric, are then merged until the entire ventricular mesh belongs to a single cluster. On this hierarchy model, the optimization starts at the root as a global parameter estimation, and progressively moves to a higher level of resolution. Each level of optimization consists of two primary tasks: 1) optimization exploiting the lower-level solution (section 3.3); and 2) determine the tree structure for the next level of optimization (section 3.2).

3.2 Adaptive Spatial Refinement: Instead of uniform resolution, we aim for a spatially-adaptive resolution so that higher resolution is only used at regions of heterogeneous tissues. In other words, instead of splitting all leaf nodes after each level of optimization, selective splitting and retraction are used to generate a skewed tree with branches only expanding into heterogeneous clusters.

The key task here is to properly identify the clusters that are heterogeneous versus homogeneous in tissue properties. Intuitively, if a cluster is homogeneous, its split is expected to yield children clusters with similar parameter values, *i.e.*, there will be minimal gain in the objective function (2). The contrary is true for heterogeneous clusters. Therefore, we propose a criteria based on gains in the objective function for adaptive spatial refinement and coarsening

Specifically, after obtaining an optimal solution $\mathbf{x}^k$ at level k, we examine two types of leaf nodes. First, we examine each pair of sibling nodes $(x^k_{i,c1}, x^k_{i,c2})$ that share the same parent node x^{k-1}_i, where $i = 1, \cdots, p$, p = the number of leaf nodes on the tree structure at level $k-1$. For each pair of $(x^k_{i,c1}, x^k_{i,c2})$, we evaluate the gain of splitting them from their parent as the difference in objective function evaluated on $\mathbf{x}^k$ versus replacing $(x^k_{i,c1}, x^k_{i,c2})$ with their parent x^{k-1}_i:

$$r_{k,i} = G(\mathbf{x}^k) - G(\mathbf{s}^k), \quad \text{where} \quad \mathbf{s}^k = (\mathbf{x}^k \setminus (x^k_{i,c1}, x^k_{i,c2}), x^{k-1}_i) \tag{3}$$

Second, for leaf nodes that do not have a sibling leaf node, no resolution change has occurred but their values may have been changed as a result of resolution-change elsewhere. For such a node x^k_i, its gain $r_{k,i}$ equals the change in the objective function due to the change in x^k_i before and after the optimization.

Based on $r_{k,i}$, two actions are taken to grow the tree for the next level of optimization: 1) for the leaf node or the pair of leaf nodes with the maximum gain $r_{k,i}$, we consider them to represent highly heterogeneous regions and warrant a higher-solution representation (*i.e.*, a split); and 2) for those that bring negligible or negative gain ($r_{k,i} < \delta$, δ is the same tolerance for the convergence of the overall framework), we decide that the split suggested by the previous level of optimization is not beneficial and retract it. The rest of the leaf nodes are kept.

3.3 Optimization via Surrogate Models: The proposed framework can be used in combination with any optimization method suitable for handling a complex objective function like (2). In this paper, a surrogate model based method using the GP is used [7]. In brief, the optimization assumes a prior distribution, in the form of a GP $\sim \mathcal{N}(\mu(\mathbf{x}), \sigma(\mathbf{x}))$, to denote the belief over the objective function (2) and sequentially updates the prior based on new data to better approximate the objective function, especially in the region of global optimum.

While the GP-based optimization is gaining increasing attention for optimizing highly expensive cost functions, it suffers from an inability to scale in high dimension: existing GP-based optimization is only effective in handling up to $10-15$ number of unknowns [7]. Here, we elaborate how the presented framework uses low-resolution solutions to facilitate the higher-resolution GP optimization. Optimization at each level of resolution consists of three main steps:

1. Initialize the GP: We start with a GP with zero mean and "Matern 5/2" covariance function [7] to impose a minimal assumption of smoothness over the objective function (2). The initial knowledge of the GP plays an important role in determining how fast a good GP surrogate can be obtained in the subsequent updates. Within the proposed framework, a set of higher-resolution points are generated from the previous lower-resolution results through a convolution operator. These points serve to quickly generate a low-resolution profile of the GP.

2. Determine the next query point: To update the GP, the best point to query should both exploit the current GP model at the solution space where predictive mean $\mu(\mathbf{x})$ is high, and explore the solution space where the predictive uncertainty $\sigma(\mathbf{x})$ is high. This is done by finding the point that maximizes the upper confidence bound $\mu(\mathbf{x}) + \kappa\sigma(\mathbf{x})$ of the GP model [7], using the BOBYQA [6] algorithm. The parameter κ balances between exploitation and exploration.

3. Update the GP: On the new query point, the objective function (2) is evaluated and the posterior distribution of the GP is updated based on the standard Bayes rule [7]. Steps 2 and 3 run in iteration until convergence.

In summary, by initializing the GP from a coarser-scale profile and by increasing resolution only at regions of heterogeneity, this entire framework can be interpreted as a progressive coarse-to-fine tuning of a GP model, with progressively higher resolution focused at regions likely to contain the global optimum.

4 Experiments

Synthetic Experiments: In a set of 22 synthetic experiments conducted on 3 image-derived realistic human heart-torso models, we test the proposed method in estimating the excitability of ventricles with infarcted tissues of varying locations and sizes. The parameter "a" of the AP model (1) is set to be 0.15 ± 0.01 and 0.45 ± 0.01, respectively, for normal and infracted tissues. 120-lead ECG are simulated and corrupted with 20dB Gaussian noise for parameter estimation. The infarct is set at different LV and RV locations using various combinations of the AHA segments, as well as random initializations with sizes smaller than one AHA segment. The infarct size ranges from 1% to 40% of the ventricles.

The presented method is compared with the BOBYQA method [6] carried out on a fixed 18-segment model (17 LV AHA segments + 1 RV segment) [9]. Because GP-based optimization did not scale well to this 18-dimensional optimization in our experiments, it is not included in this paper. We evaluate the estimated parameters using two metrics: 1) root mean square error (RMSE) between the true and estimated parameters; and 2) dice coefficient (DC) $= \frac{2|S_1 \cap S_2|}{|S_1|+|S_2|}$, where S_1 and S_2 are the sets of cardiac nodes in the true and estimated regions of infarct; these regions are defined from the final tree structure in the presented method,

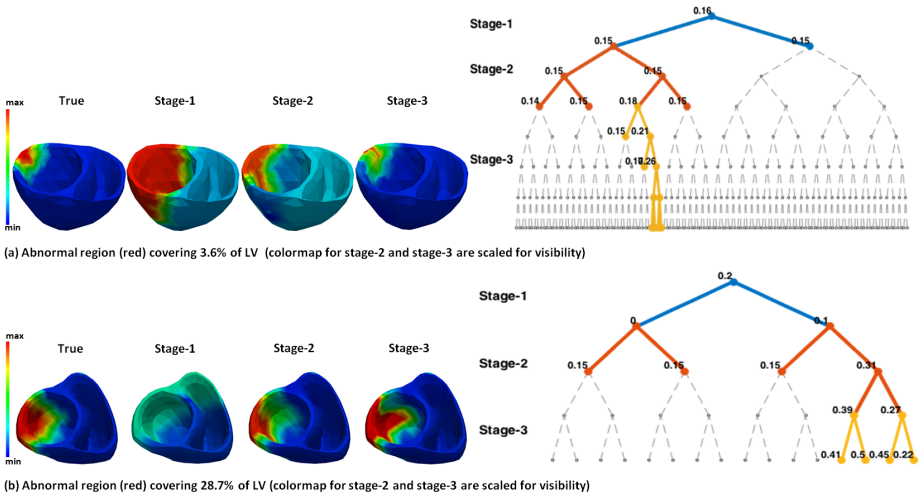

Fig. 1: Examples of the progression of the coarse-to-fine optimization method. Left: true parameter settings *vs.* estimation results improved over 3 successive stages of the optimization. Right: the corresponding growth of the tree at each stage. The gray, dotted structure shows the hierarchy model, whereas the colored line demonstrates the path taken by the spatially-adaptive optimization method.

and by thresholding estimated parameter values in the BOBYQA method. Both metrics are evaluated at the resolution of the cardiac mesh.

Fig. 1 demonstrates how the presented coarse-to-fine optimization progresses: the left panel shows the improvement of estimation at 3 successive stages of the optimization, with the corresponding growth of the tree illustrated in the right panel. Fig. 1a shows an example on a small infarct (3%). The tree growth shows that since stage 1, the optimization split only along the heterogeneous region that contains the abnormal tissue. It continued narrowing down the infarct with higher resolution until convergence, generating a narrow yet deep tree. The accurate result shown in stage 3 of Fig. 1a was achieved with only a dimension of 10 unknowns. In comparison, if a uniform resolution is used, a minimal dimension of 128 is needed to achieve the same resolution. Fig. 1b shows another example with a larger infarct (29%). Because abnormal tissues span a larger number of clusters compared to a small infarct, it is not until stage 2 before the tree can be split along one major branch. In addition, because both normal and abnormal tissues are large enough to be represented by low-resolution, homogeneous regions, an overall lower-resolution solution is obtained with a wider yet shallow tree. A uniform resolution in this case will require a dimension of 16, while the presented method converged at a dimension of 7.

Fig. 2 summarizes the comparison between the presented method and the BOBYQA method directly carried out on the fixed 18-segment model. The improvement of the presented method is statistically significant in both DC and RMSE (paired-t tests, $p < 0.001$). More specifically, the performance of the presented method is much more robust to the size and distribution/shape of

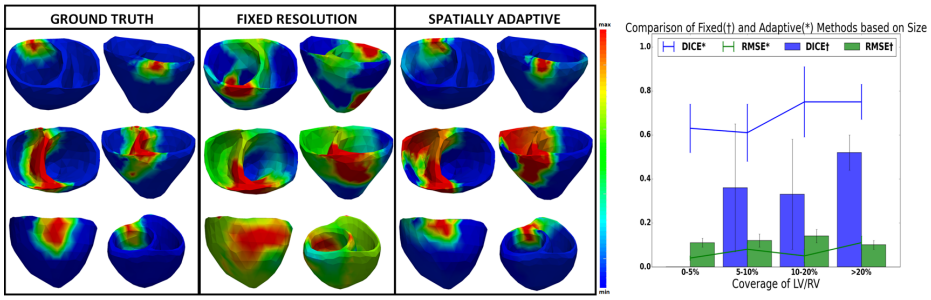

Fig. 2: Comparison of the presented method with BOBYQA on a 18-segment model. Left: examples of different infarcts. Right: quantitative comparison in DC and RMSE.

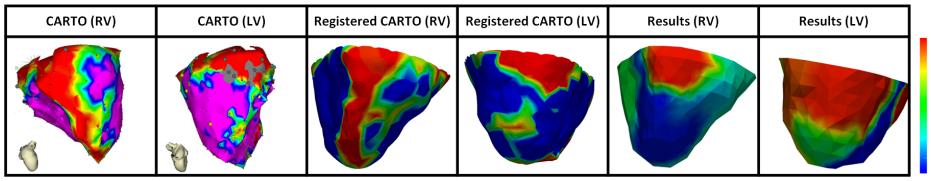

Fig. 3: Real-data experiment: comparison with *in-vivo* voltage maps of scar.

the infarct. While optimization on fixed segments has trouble handling infarcts of size equal to a single AHA segment, the presented method could provide an accurate estimation using only 10-14 dimensions of unknowns. Furthermore, optimization on fixed segments tends to show false-positives across multiple segments, falling short to reveal the spatial distribution of an infarct. The presented method improve this accuracy by adaptively focusing higher-resolution on the boundary between homogeneous healthy and infarct regions.

Real-Data Experiment: As a feasibility test, we conducted a case study on a patient who underwent catheter ablation of ventricular tachycardia due to prior tissue infraction. Tissue excitability was estimated from 120-lead ECG on the patient-specific heart-torso geometry obtained from CT images. Bipolar voltage data obtained during *in-vivo* CARTO mapping were used as reference data: as illustrated in Fig. 3, they reveal low-voltage regions at both lateral LV and RV (red: dense scar $\leq$0.5mV; green: scar border = 0.5-1.5 mV; blue: normal >1.5mV). Excitability estimated from the presented framework successfully captured abnormal tissues at both locations. Interestingly, in post-processing of CARTO maps, it was noted by the clinician that the low-voltage region at middle-apical lateral RV was caused by poor catheter contact rather than scar tissue. The estimated excitability values, therefore, revealed a more accurate representation of the tissue property than *in-vivo* catheter maps. Overall, the core and border of abnormal tissues as revealed by the estimated excitability appear to co-locate well with CARTO maps. It is noteworthy that, because CARTO maps show voltage data whereas the estimated parameter map show tissue excitability, they are not expected to appear identical; further caution is needed in interpreting the CARTO data due to its inherent uncertainty.

Conclusion: This paper presents a novel framework that is able to achieve a higher-resolution local parameter estimation using a small number of unknowns. This is enabled by a coarse-to-fine optimization, and a spatially-adaptive resolution that is higher at heterogeneous regions (*e.g.*, infarct border) and lower at homogeneous regions (*e.g.*, healthy tissue and infarct core). Theoretically, when needed, the proposed method has the potential to go down the tree until it reaches the final resolution of individual cardiac nodes. As shown in the presented experiments, however, the estimation accuracy is limited around the infarct border at the current stage. An important next step, therefore, is to improve the ability of the presented algorithm to go deeper along the tree, overcoming the associated computation and observability issues. In addition, it is desirable to incorporate probabilistic estimation into the framework and to investigate the influence of different algorithm parameters on its performance.

References

1. Chinchapatnam, P., Rhode, K.S., Ginks, M., Rinaldi, C.A., Lambiase, P., Razavi, R., Arridge, S., Sermesant, M.: Model-based imaging of cardiac apparent conductivity and local conduction velocity for diagnosis and planning of therapy. Medical Imaging, IEEE Transactions on 27(11), 1631–1642 (2008)
2. Clayton, R., Panfilov, A.: A guide to modelling cardiac electrical activity in anatomically detailed ventricles. Progress in biophysics and molecular biology 96(1), 19–43 (2008)
3. Hastie, T., Tibshirani, R., Friedman, J.: Unsupervised learning. Springer (2009)
4. Konukoglu, E., Relan, J., Cilingir, U., Menze, B.H., Chinchapatnam, P., Jadidi, A., Cochet, H., Hocini, M., Delingette, H., Jaïs, P., et al.: Efficient probabilistic model personalization integrating uncertainty on data and parameters: Application to eikonal-diffusion models in cardiac electrophysiology. Progress in biophysics and molecular biology 107(1), 134–146 (2011)
5. Lê, M., Delingette, H., Kalpathy-Cramer, J., Gerstner, E.R., Batchelor, T., Unkelbach, J., Ayache, N.: Bayesian personalization of brain tumor growth model. In: MICCAI, 2015
6. Powell, M.J.: The bobyqa algorithm for bound constrained optimization without derivatives. Cambridge NA Report NA2009/06, University of Cambridge, Cambridge (2009)
7. Shahriari, B., Swersky, K., Wang, Z., Adams, R.P., de Freitas, N.: Taking the human out of the loop: A review of bayesian optimization. Proceedings of the IEEE 104(1), 148–175 (2016)
8. Wang, L., Zhang, H., Wong, K.C., Liu, H., Shi, P.: Physiological-model-constrained noninvasive reconstruction of volumetric myocardial transmembrane potentials. Biomedical Engineering, IEEE Transactions on 57(2), 296–315 (2010)
9. Wong, K.C., Sermesant, M., Rhode, K., Ginks, M., Rinaldi, C.A., Razavi, R., Delingette, H., Ayache, N.: Velocity-based cardiac contractility personalization from images using derivative-free optimization. Journal of the mechanical behavior of biomedical materials 43, 35–52 (2015)
10. Zettinig, O., Mansi, T., Georgescu, B., Kayvanpour, E., Sedaghat-Hamedani, F., Amr, A., Haas, J., Steen, H., Meder, B., Katus, H., et al.: Fast data-driven calibration of a cardiac electrophysiology model from images and ecg. In: MICCAI, 2013